Aalto University

OPEN ACCESS

This is an electronic reprint of the original article.
This reprint may differ from the original in pagination and typographic detail.

Alaee, R.; Albooyeh, M.; Yazdi, M.; Komjani, N.; Simovski, C.; Lederer, F.; Rockstuhl, C.

Magneto-electric coupling in nonidentical plasmonic nanoparticles: Theory and applications

Published in:
Physical Review B

DOI:
10.1103/PhysRevB.91.115119

Published: 01/01/2015

Document Version
Publisher's PDF, also known as Version of record

Please cite the original version:
Alaee, R., Albooyeh, M., Yazdi, M., Komjani, N., Simovski, C., Lederer, F., & Rockstuhl, C. (2015). Magneto-electric coupling in nonidentical plasmonic nanoparticles: Theory and applications. *Physical Review B*, *91*(11), 1-8. Article 115119. https://doi.org/10.1103/PhysRevB.91.115119

This material is protected by copyright and other intellectual property rights, and duplication or sale of all or part of any of the repository collections is not permitted, except that material may be duplicated by you for your research use or educational purposes in electronic or print form. You must obtain permission for any other use. Electronic or print copies may not be offered, whether for sale or otherwise to anyone who is not an authorised user.

Magnetoelectric coupling in nonidentical plasmonic nanoparticles: Theory and applications

R. Alaee,[1,*] M. Albooyeh,[2,*] M. Yazdi,[3] N. Komjani,[3] C. Simovski,[2] F. Lederer,[4] and C. Rockstuhl[1,5]
[1]*Institute of Theoretical Solid State Physics, Karlsruhe Institute of Technology, Karlsruhe, Germany*
[2]*Department of Radio Science and Engineering, Aalto University, Espoo, Finland*
[3]*Electrical Engineering Department, Iran University of Science and Technology, Tehran, Iran*
[4]*Institute of Condensed Matter Theory and Solid State Optics, Abbe Center of Photonics, Friedrich-Schiller-Universität Jena, Jena, Germany*
[5]*Institute of Nanotechnology, Karlsruhe Institute of Technology, Karlsruhe, Germany*

(Received 18 November 2014; revised manuscript received 20 February 2015; published 10 March 2015)

We explore the optical properties of a meta-atom made of plasmonic nanopatches that possess an increasing degree of complexity. We show that if two nanopatches are strongly coupled and have a different geometrical footprint, the meta-atom exhibits a resonant magnetoelectric response, in addition to the anticipated resonant electric and magnetic response. Thus, it behaves similarly as the so-called omega particle, but with the unique advantage that frequency and strength of this magnetoelectric resonance can be independently tuned and modified with respect to the corresponding values of the electric resonance. This allows a metasurface of such meta-atoms to possess widely controlled reflection and transmission coefficients, e.g., the regimes of strongly asymmetric reflectance and perfect absorption become possible. Alternatively, an individual meta-atom of such kind can act as a directive nanoantenna with zero backscattered fields (Huygens' scatterer).

DOI: 10.1103/PhysRevB.91.115119 PACS number(s): 42.25.−p, 42.70.−a, 78.67.Bf, 78.20.Bh

I. INTRODUCTION

Planar metamaterials, called herein metasurfaces, promise to control the propagation of light just as their bulk counterparts [1,2]. However, metasurfaces benefit from the additional advantage of being less lossy. With the ability to realize metasurfaces by using modern fabrication technologies, it is by no surprise that they draw the attention of the research community [3–9]. This holds especially for metasurfaces designed to operate at visible frequencies where many promising applications are in reach [10–13]. However, especially if it concerns the optical domain, it is of utmost importance that the geometry of the unit cells from which the metasurfaces are composed of, i.e., the meta-atoms, are as simple as possible to adhere to the requirements of practical fabrication technologies. This, naturally, led to the tendency to make the meta-atoms from rather simple elements such as patches, disks, strips, spheres, cylinders, and rings [14–21]. A meta-atom can be formed by such a simple single element: then metasurfaces consisting of such meta-atoms possess electric resonances only. A meta-atom consisting of a pair of such moieties possesses also a resonant magnetic response [21–26]. For example, it has been shown that a metasurface of nanopatches has an electric resonance [27,28] while two coupled nanopatches have both electric and magnetic resonances [21,23–26]. It is easy to appreciate that a metasurface possessing either an electric or a magnetic response provides less control on optical responses [29] when compared with a metasurface possessing simultaneously both electric and magnetic responses (Huygens' metasurface) [30–32].

An even higher control of the optical response is possible while exploiting the magnetoelectric bianisotropy effect. Bianisotropy is related to an electric/magnetic response to a magnetic/electric excitation [33–36]. This effect inherently causes an asymmetry in the metasurface response if illuminated from different directions. Depending on the specific kind of bianisotropy, the asymmetry may occur in reflection, transmission, or in both [34,37]. There are many applications associated with this basic effect. For example, it is possible to polarize incident waves [38,39] or to make a sheet transparent from one direction while being fully opaque from the other [40]. Indeed, when higher order multipole moments are absent in the response of the meta-atoms, bianisotropy provides the most comprehensive control of the reflection and transmission spectra [33].

However, the question always arises on how the actual meta-atom has to look to provide such bianisotropic response. Solutions suggested thus far usually rely on involved geometries which are challenging to fabricate at optical frequencies [33,37,39]. Moreover, in most cases only a single resonant mode is exploited. This mode may possess an electric, magnetic, and magnetoelectric contribution, but they all naturally share the same resonance frequencies. This significantly limits the degree of freedom in the design while a more independent control is highly desirable. Only with that, the magnitude of the different contributions could be suitably adjusted for specific applications.

To solve this problem we demonstrate here a viable route to achieve the desired bianisotropic response with a meta-atom that is easy to fabricate. Most importantly, for the meta-atom we discuss, the frequency of magnetoelectric resonance is independent to the electric one, which allows the observation of intriguing effects.

The paper is divided into two parts. First, we theoretically discuss the optical properties of a meta-atom made from nanopatches. We consider these properties with increasing geometrical complexity and demonstrate how to unlock specific optical responses. The eventual meta-atom consists of two closely spaced metallic nanopatches with a different

*Equally contributed to the work. Corresponding author: rasoul.khanghah@kit.edu

 ©2015 American Physical Society

geometrical footprint that provides the desired bianisotropic response. The optical response of the isolated meta-atom is discussed but also the reflection and transmission from a metasurface thereof. Second, different applications are studied. They are explored on phenomenological grounds where the necessary optical properties are outlined concerning the magnetoelectric response to achieve a specific effect. Then, using full wave simulations, it is demonstrated that these effects can indeed be observed with the meta-atom under consideration.

II. OPTICAL RESPONSE OF A DENSE RESONANT ARRAY AT NORMAL INCIDENCE

The purpose of this section is to provide a concise overview on how the optical response of a metasurface made from periodically arranged meta-atoms is calculated [33,37,41,42]. The meta-atom will be described with a bianisotropic polarizability tensor.

Let us first consider a metasurface consisting of an optically dense planar array (square two-dimensional grid) of optically small resonant particles embedded in a uniform host medium. We assume air throughout the work as the host medium but any other dielectric environment can easily be considered. Moreover, we assume that the array is uniaxial in its plane, i.e., the optical response will be preserved if we modify the polarization of the incident field around the line normal to the plane. The array is placed in the xy plane and the period a is sufficiently small [41] compared to the incident wavelength λ in the host medium. Without loss of generality, we assume that the metasurface is illuminated by an x-polarized monochromatic plane wave at normal incidence. Thus, its electric field can be written as $\mathbf{E}^{\mathrm{i}}(\mathbf{r},t) = \mathbf{e}_x E_{\mathrm{x}}^{\mathrm{i}} \exp(j\omega t)\exp(\mp jk_z z)$. Here $\mathbf{e}_x$ is the unit vector in the x direction, k_z is the propagation constant along the z axis, ω is the angular frequency, and $E_{\mathrm{x}}^{\mathrm{i}}$ is the electric field amplitude in the x direction. The field can propagate in a forward $(-)$ or backward $(+)$ direction depending on the chosen sign.

In our contribution we only consider electric and magnetic dipole moments of meta-atoms, neglecting quadrupoles and higher-order moments [43–47]. That is, we are interested in the case when both electric and magnetic moments are induced by local electric and magnetic fields. Therefore, the relations between induced electric dipole moment vector $\mathbf{p} = (p_{\mathrm{x}}, p_{\mathrm{y}}, p_{\mathrm{z}})$, magnetic dipole moment vector $\mathbf{m} = (m_{\mathrm{x}}, m_{\mathrm{y}}, m_{\mathrm{z}})$, and the incident field $\{\mathbf{E}^{\mathrm{i}} = (E_{\mathrm{x}}^{\mathrm{i}},0,0), \mathbf{H}^{\mathrm{i}} = (0,H_{\mathrm{y}}^{\mathrm{i}},0)\}$ read as [48]

$$\begin{aligned} \mathbf{p} &= \bar{\bar{\alpha}}^{\mathrm{ee}}\mathbf{E}^{\mathrm{loc}} + \bar{\bar{\alpha}}^{\mathrm{em}}\mathbf{H}^{\mathrm{loc}}, \\ \mathbf{m} &= \bar{\bar{\alpha}}^{\mathrm{me}}\mathbf{E}^{\mathrm{loc}} + \bar{\bar{\alpha}}^{\mathrm{mm}}\mathbf{H}^{\mathrm{loc}}, \end{aligned} \tag{1}$$

where $\mathbf{E}^{\mathrm{loc}} = \mathbf{E}^{\mathrm{i}} + \bar{\bar{\beta}}^{\mathrm{ee}}\mathbf{p}$ and $\mathbf{H}^{\mathrm{loc}} = \mathbf{H}^{\mathrm{i}} + \bar{\bar{\beta}}^{\mathrm{mm}}\mathbf{m}$. Here $\bar{\bar{\alpha}}^{\mathrm{ee}}/\bar{\bar{\alpha}}^{\mathrm{mm}}$ and $\bar{\bar{\alpha}}^{\mathrm{em}}/\bar{\bar{\alpha}}^{\mathrm{me}}$ are the electric/magnetic and electromagnetic/magnetoelectric polarizability dyadic of individual meta-atoms, respectively. Parameters $\bar{\bar{\beta}}^{\mathrm{ee}}$ and $\bar{\bar{\beta}}^{\mathrm{mm}}$ are called interaction constants. They measure contributions of the fields created by all other particles of the array to the local fields $\bar{\mathbf{E}}^{\mathrm{loc}}$ and $\bar{\mathbf{H}}^{\mathrm{loc}}$ exciting each meta-atom (see, e.g., Ref. [41]). The interaction constants for electric and magnetic dipoles are calculated in [41,42,49] for different dipole arrangements.

We are only interested in the reciprocal omega (Ω) type bianisotropy such that other bianisotropy types, i.e., chiral, Tellegen, and "moving" are absent [33]. Omega-type bianisotropy refers to the case when $\bar{\bar{\alpha}}^{\mathrm{em}} = -(\bar{\bar{\alpha}}^{\mathrm{me}})^T$ [33]. For an x-polarized illumination such omega particles preserve the polarization and no cross-polarized dipole moments are induced [33], i.e., $p_{\mathrm{y}} = p_{\mathrm{z}} = 0$ and $m_{\mathrm{x}} = m_{\mathrm{z}} = 0$. This can be easily assured by choosing a proper arrangement of the meta-atoms in the array with respect to the incidence polarization. Consequently, scalar moments p_{x} and m_{y} and scalar polarizabilities $\alpha_{\mathrm{xx}}^{\mathrm{ee}}$, $\alpha_{\mathrm{yy}}^{\mathrm{mm}}$, $\alpha_{\mathrm{xy}}^{\mathrm{em}}$, and $\alpha_{\mathrm{yx}}^{\mathrm{me}}$ are the only components appearing in (1), i.e.,

$$\begin{aligned} p_{\mathrm{x}} &= \alpha_{\mathrm{xx}}^{\mathrm{ee}} E_{\mathrm{x}}^{\mathrm{loc}} + \alpha_{\mathrm{xy}}^{\mathrm{em}} H_{\mathrm{y}}^{\mathrm{loc}}, \\ m_{\mathrm{y}} &= \alpha_{\mathrm{yx}}^{\mathrm{me}} E_{\mathrm{x}}^{\mathrm{loc}} + \alpha_{\mathrm{yy}}^{\mathrm{mm}} H_{\mathrm{y}}^{\mathrm{loc}}, \end{aligned} \tag{2}$$

where $E_{\mathrm{x}}^{\mathrm{loc}} = E_{\mathrm{x}}^{\mathrm{i}} + \beta^{\mathrm{ee}} p_{\mathrm{x}}$ and $H_{\mathrm{y}}^{\mathrm{loc}} = H_{\mathrm{y}}^{\mathrm{i}} + \beta^{\mathrm{mm}} m_{\mathrm{y}}$. On the other hand, the reflected $E_{\mathrm{x}}^{\mathrm{r}}$ and transmitted $E_{\mathrm{x}}^{\mathrm{t}}$ electric fields in terms of electric and magnetic dipole moments may be written as [39]

$$\begin{aligned} E_{\mathrm{x}}^{\mathrm{r}} &= \frac{-j\omega}{2a^2}[\eta p_{\mathrm{x}} \mp m_{\mathrm{y}}], \\ E_{\mathrm{x}}^{\mathrm{t}} &= E_{\mathrm{x}}^{\mathrm{i}} - \frac{j\omega}{2a^2}[\eta p_{\mathrm{x}} \pm m_{\mathrm{y}}], \end{aligned} \tag{3}$$

where η is the characteristic impedance in the host medium. With these assumptions and using Eqs. (2) and (3), the reflection and transmission coefficients for an omega-type bianisotropic uniaxial array read as

$$r = \frac{E_{\mathrm{x}}^{\mathrm{r}}}{E_{\mathrm{x}}^{\mathrm{i}}} = \frac{-j\omega}{2a^2\Delta}\left[\eta\alpha_{\mathrm{xx}}^{\mathrm{ee}} \pm \alpha_{\mathrm{xy}}^{\mathrm{em}} \mp \alpha_{\mathrm{yx}}^{\mathrm{me}} - \frac{1}{\eta}\alpha_{\mathrm{yy}}^{\mathrm{mm}}\right], \tag{4a}$$

$$\begin{aligned} t = \frac{E_{\mathrm{x}}^{\mathrm{r}}}{E_{\mathrm{x}}^{\mathrm{i}}} = 1 - \frac{j\omega}{2a^2\Delta}\Bigg[&\eta\alpha_{\mathrm{xx}}^{\mathrm{ee}} \pm \alpha_{\mathrm{xy}}^{\mathrm{em}} \pm \alpha_{\mathrm{yx}}^{\mathrm{me}} + \frac{1}{\eta}\alpha_{\mathrm{yy}}^{\mathrm{mm}} \\ &- \frac{2\beta^{\mathrm{ee}}}{\eta}\left(\alpha_{\mathrm{xx}}^{\mathrm{ee}}\alpha_{\mathrm{yy}}^{\mathrm{mm}} - \alpha_{\mathrm{xy}}^{\mathrm{em}}\alpha_{\mathrm{yx}}^{\mathrm{me}}\right)\Bigg], \end{aligned} \tag{4b}$$

where $\Delta = 1 - \alpha_{\mathrm{xx}}^{\mathrm{ee}}\beta^{\mathrm{ee}} - \alpha_{\mathrm{yy}}^{\mathrm{mm}}\beta^{\mathrm{mm}} - (\alpha_{\mathrm{xy}}^{\mathrm{em}}\alpha_{\mathrm{yx}}^{\mathrm{me}} - \alpha_{\mathrm{xx}}^{\mathrm{ee}}\alpha_{\mathrm{yy}}^{\mathrm{mm}})\beta^{\mathrm{ee}}\beta^{\mathrm{mm}}$. Notice that for an isotropic array with omega particles at normal incidence, both the cross-polarized reflection $E_{\mathrm{y}}^{\mathrm{r}}/E_{\mathrm{x}}^{\mathrm{i}}$ and transmission $E_{\mathrm{y}}^{\mathrm{t}}/E_{\mathrm{x}}^{\mathrm{i}}$ vanish. In order to find the reflection and transmission coefficients for a metasurface made from specific meta-atoms, we first determine the individual polarizability components $\alpha_{\mathrm{xx}}^{\mathrm{ee}}$, $\alpha_{\mathrm{yy}}^{\mathrm{mm}}$, $\alpha_{\mathrm{xy}}^{\mathrm{em}}$, and $\alpha_{\mathrm{yx}}^{\mathrm{me}}$ with the help of the multipole expansion of scattered fields described in Refs. [43,45] and the method explained in Refs. [45,50,51]. The approach to retrieve all polarizability components is briefly outlined in the following. First, we illuminate the meta-atom with a plane wave ($E_{\mathrm{x}}^{\mathrm{i}} = 1$ V/m, $H_{\mathrm{y}}^{\mathrm{i}} = \pm E_{\mathrm{x}}^{\mathrm{i}}/\eta$) from two opposite directions $(\pm)$. Then, the electric and magnetic dipolar moments for these two scenarios ($p_{\mathrm{x}}^{\pm}$, $m_{\mathrm{y}}^{\pm}$) are calculated. This is done by projecting the scattered electromagnetic fields from each configuration to the field of an electric and magnetic dipole that is situated in the central coordinate [43,45,52]. Finally, all polarizability components can be expressed as [51]

$$
\begin{aligned}
\alpha_{\mathrm{xx}}^{\mathrm{ee}} &= \frac{(p_{\mathrm{x}}^{+} + p_{\mathrm{x}}^{-})}{2},\\
\alpha_{\mathrm{xy}}^{\mathrm{em}} &= \frac{(p_{\mathrm{x}}^{+} - p_{\mathrm{x}}^{-})}{2}\eta,\\
\alpha_{\mathrm{yx}}^{\mathrm{me}} &= \frac{(m_{\mathrm{y}}^{+} + m_{\mathrm{y}}^{-})}{2},\\
\alpha_{\mathrm{yy}}^{\mathrm{mm}} &= \frac{(m_{\mathrm{y}}^{+} - m_{\mathrm{y}}^{-})}{2}\eta.
\end{aligned}
\tag{5}
$$

Thereafter, calculating the interaction constants β^{ee} and β^{mm} from Ref. [41] and using Eqs. (4) one may finally find the reflection and transmission coefficients. Notice, the last expressions in Eqs. (4) are important since they allow us to discuss the scattering properties of a general omega-type bianisotropic array using the properties of its individual constituents and the interaction between them. In the following we discuss the achievable optical response of a metasurface made of meta-atoms with increasing complexity.

III. OPTICAL PROPERTIES OF META-ATOMS

A. Single nanopatches

We start with the simplest design that has been previously widely studied [27]. That is a gold nanopatch as shown in Fig. 1(a). This gold nanopatch sustains an electric resonance in response to an incident electromagnetic field whenever a localized surface plasmon polariton is excited [Fig. 1(g)]. As a result, a metasurface composed of nanopatches will provide an electric resonance behavior in response to a plane wave illumination. That is, except for the electric polarizability $\alpha_{\mathrm{xx}}^{\mathrm{ee}}$, all other polarizability components in (4) are zero. Therefore, this electric resonance is the only mechanism which can be used to control the optical response of the metasurface. The array response can be controlled [Fig. 1(d)] by changing the distance between the particles, i.e., interaction constants β^{ee} and the patch dimensions, i.e., resonance frequency of the

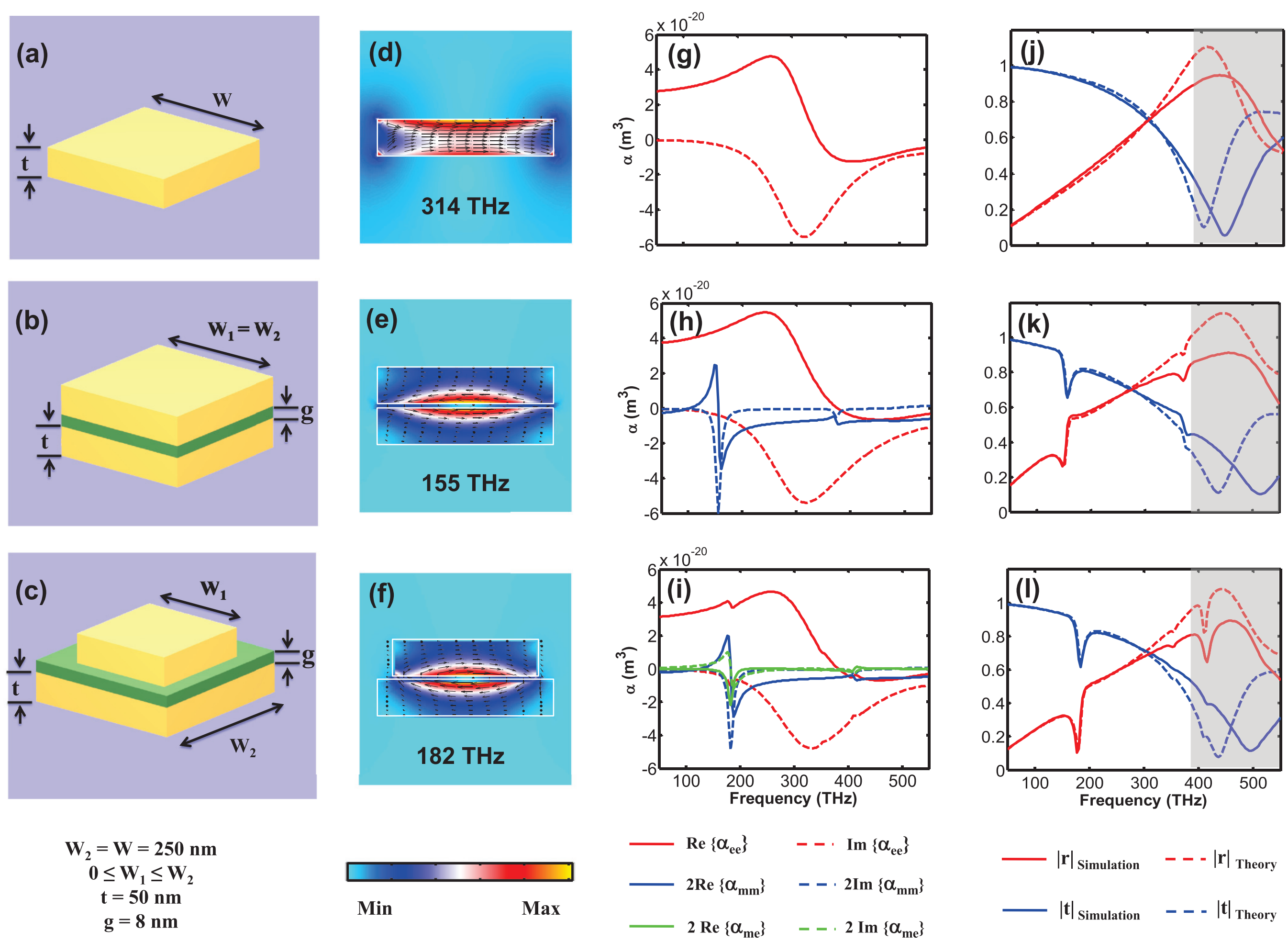

FIG. 1. (Color online) Schematic representation of relevant meta-atoms. (a) A single nanopatch, (b) two identical nanopatches, and (c) two coupled nonidentical nanopatches. (d), (e), and (f) Current distributions at frequencies of interest. (g), (h), and (i) Semianalytically extracted polarizability components of each meta-atom (sketched in the same unit, i.e., m^3). (j), (k), and (l) Full wave simulation and analytical results for reflection and transmission spectra of metasurfaces made of these meta-atoms. Geometrical details of the meta-atom are given in the lower left corner of the figure. The periodicity is always chosen to be $a = 400$ nm, the dielectric spacer has a refractive index of $n = 1.46$ in (b) and (c), and $W_1 = 200$ nm was chosen in (c). Ambient material is air.

particles [Figs. 1(g) and 1(j)]. However, with such simple nanopatches, only very limited control on the level of reflection and transmission spectra can be achieved. Moreover, the optical response of the array is identical if illuminated from either direction.

B. Identical coupled nanopatches

It is evident from (4) that an additional magnetic response permits more control on the reflection and transmission. This is feasible in a next step by adding an identical, closely spaced nanopatch on top of the first one [Fig. 1(b)]. As shown in Fig. 1(h), in addition to the previous electric resonance, a new magnetic one is now supported by the coupled nanopatch. This occurs due to the hybridization of the modes, sustained by the individual nanopatches, to form an antisymmetric (bonding, low energy) and a symmetric (antibonding, high energy) mode. The antisymmetric mode [current distribution is shown in Fig. 1(e)] evokes the magnetic response. This can be recognized from the particle polarizabilities shown in Fig. 1(h). However, bianisotropy remains absent in such coupling scheme. Therefore, α_{xy}^{em} and α_{yx}^{me} are still zero in (4).

Similar structures like the present one, such as nanodisks, are widely used in the literature as one of the simplest building blocks in periodic arrays to obtain a magnetic response [16,24,25]. In dipole approximation, both strength and frequency of the magnetic resonance can be tuned by varying the distance between both nanopatches. However, the magnetic resonance is always spectrally separated from the electric one. Therefore, although the magnitude of the achievable electric polarization at the magnetic resonance is comparable to the magnetic polarization, it is not possible to balance the scattering contribution from the different dipole polarizabilities. Moreover, according to (4) there is still no control of the directional scattering response, i.e., the array behaves identically for forward and backward illumination directions.

C. Nonidentical coupled nanopatches

To obtain even better control on the specific optical spectra as well as to achieve a directional dependent response, the symmetry of the structure has to be broken. With that, a notable bianisotropic effect is in reach, i.e., a dispersion in α_{xy}^{em} and α_{yx}^{me}. Having nonzero values for these coefficients renders the optical coefficients r and t [Eqs. (4)] to be functions of four complex polarizability components instead of only two as previously considered. This naturally increases the degrees of freedom. Moreover, it is clear from Eqs. (4) that due to the different signs of α_{xy}^{em} and α_{yx}^{me} a different optical response is obtained while illuminating the samples from different directions. An important design criterion will be that the coefficients α_{xy}^{em} and α_{yx}^{me} should exhibit a comparable strength as the electric and magnetic polarizabilities at the same frequencies rather than being only nonzero.

To achieve such a notable bianisotropy, point of departure is the same double nanopatch topology as before but now with different lateral dimensions of the nanopatches [Fig. 1(c)]. In passing, we note that this response is different from the magnetoelectric response created by a wire omega particle [53]. Therefore, the resonance frequencies for the dispersion in all polarizabilities, i.e., the electric, magnetic, and magnetoelectric mode, are identical since they are linked to the same mode sustained by the particle [53]. In contrast, the magnetic and the magnetoelectric resonance frequencies are identical here but the electric resonance is different. However, since the magnetic and electric dipole moments which are created by the electric and magnetic fields in the plane of the array, respectively, are perpendicular to each other, the presented double patch scheme can be generally considered as an Ω-type particle as well [33].

It is clear from Fig. 1(f) that the current distribution of this structure shown at the low frequency resonance produces a magnetic response, comparable to the situation of identical nanopatches [Fig. 1(e)]. However, for nonidentical nanopatches the circulating currents are no longer symmetric with respect to the geometrical origin of these two nanopatches. This results in a magnetoelectric/electromagnetic response. As can be expected from Eqs. (4), the reciprocity evoked asymmetry $\alpha_{xy}^{em} = -\alpha_{yx}^{me}$ yields different reflection spectra if illuminated from the opposite direction [Figs. 2(b) and 2(c)] while the transmissions remain equal. It is also expected to observe a maximum contrast

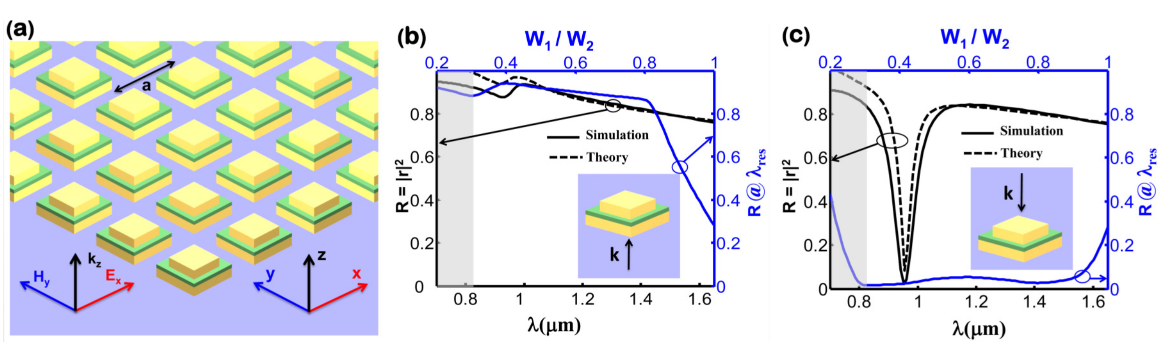

FIG. 2. (Color online) (a) Geometry of a typical planar array located in the xy plane composed of omega particles and illuminated by a plane wave with the electromagnetic field $\{E_x^i, H_y^i\}$. Full-wave simulations and analytical predictions for the reflection spectra (black lines) when illuminating the array with a forward (b) or a backward (c) propagating plane wave. The array is composed of nonidentical nanopatches. The ratio of W_1/W_2 is chosen to be 0.4 and the absolute size of W_2 is kept fix at 250 nm. We see a dramatically different response if the array is illuminated from different directions. In the forward direction (b) the reflection is nearly constant in the entire spectrum. In the backward direction (c) a pronounced resonance occurs with a well developed dip. By changing the ratio of W_1/W_2 the resonance frequency changes but the optical response is robust. This can be seen in the plot of the reflection at the resonance wavelength as function of this ratio (blue curves in both figures). The period of the array is fixed to be $a = 275$ nm.

between the reflection spectra for the forward and backward illuminations when $\Re\{(\eta^2\alpha_{xx}^{ee} - \alpha_{yy}^{mm})(\alpha_{yx}^{me} - \alpha_{xy}^{em})^*\}$ ($*$ denotes the complex conjugate) is maximum. However, it should be noted that the presence of losses is essential to get asymmetric reflection. A parametric study illustrated in Figs. 2(b) and 2(c) reveals that the maximum difference between the amplitude of reflection coefficients upon illumination from opposite directions occurs at a ratio of $\frac{W_1}{W_2} \approx 0.4$.

It is important to state that the analytical model presented here proves to be a very reliable tool to correctly explain the array behavior. Notice that the gray shadows in Figs. 1(j)–1(l) represent spectral domains where contributions of higher order modes are no longer negligible. Consequently, the analytical model is less predictive there. However, the model presented here is fully sufficient to explain the reflection and transmission coefficients at the desired frequency band qualitatively, but full wave simulations are necessary to quantitatively predict the optical response from the array.

To perceive applications that exploit the suggested meta-atoms, one may modify the lateral dimension of the upper nanopatch to vary strength and resonance frequency of the magnetoelectric response. With that, we may achieve interesting applications such as perfect absorption in an array [18,54–57] or a directive nanoantenna with zero backscattering [58–60]. They are demonstrated in the succeeding section.

IV. APPLICATIONS

A. Perfect absorber

We first present an interesting example for an application where light is nearly totally absorbed in a metasurface with a subwavelength thickness ($\approx\lambda/10$) at a specific resonance band. The proposed metasurface is not anymore a total reflector from the other direction far from the resonance band because it consists of an array of isolated particles rather than, as usually considered, of an array of particles on top of a metallic film. In general, complete light absorption can be achieved by suppressing transmission and reflection (i.e., $R = 0$ and $T = 0$) from one direction only. According to Eqs. (4), conditions for total absorption in terms of individual polarizability components for backward illumination can be expressed as

$$\eta\alpha_{xx}^{ee} = 2\alpha_{xy}^{em} + \frac{1}{\eta}\alpha_{yy}^{mm}, \quad (6)$$

$$\frac{2a^2\Delta}{j\omega} = \eta\alpha_{xx}^{ee} + \frac{1}{\eta}\alpha_{yy}^{mm} - \frac{2\beta^{ee}}{\eta}\left(\alpha_{xx}^{ee}\alpha_{yy}^{mm} - \alpha_{xy}^{em}\alpha_{yx}^{me}\right). \quad (7)$$

Figures 3(a) and 3(b) show the real and imaginary parts of the left and right sides of Eqs. (6) and (7) at resonance as a function of W_1/W_2 for backward illumination. It shows that the nearly total absorption regime can be achieved when both conditions are satisfied and this is indicated by the red shaded areas in Figs. 3(a) and 3(b). Figure 3(c) shows a parametric study of the maximum absorbed power (that is maximum at resonance frequency) for different ratios of $\frac{W_1}{W_2}$ with illumination from the backward direction. Note that the maximum absorption for a varying ratio of $\frac{W_1}{W_2}$ takes place at different wavelengths (λ_{max}). The wavelength dependent response for the situation where the maximum share of light is absorbed is also illustrated in Fig. 3(c). The nearly total absorption occurs for a ratio of $\frac{W_1}{W_2} \approx 0.4$ for an array period of $a = 275$ nm (g and t are fixed to be 8 and 50 nm).

It is evident from Fig. 3(c) that for an array with identical particles ($W_1 = W_2$) it is impossible to approach the perfect absorption regime. In this case the absorption is less than 50%. This is obvious, since there is only insufficient control of frequency and strength of the magnetic resonance in order to balance it with the electric resonance though both the electric and magnetic resonances are available in the grid.

Notice that for the illumination in the forward direction the absorption is very low and the array is nearly reflective at resonance [Fig. 2(b)]. It is also very interesting to mention that the presence of both magnetic and magnetoelectric couplings is essential to achieve the perfect absorption regime although

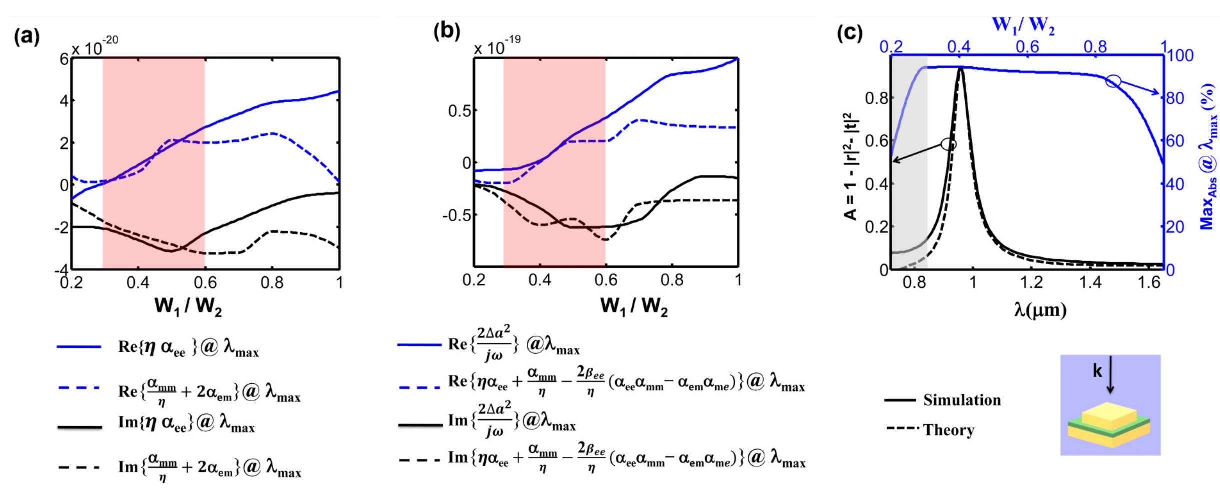

FIG. 3. (Color online) (a) and (b) The real and imaginary parts of the left and right sides of Eqs. (6) and (7) at resonance frequency as a function of W_1/W_2 for a backward illumination. The red sections represent spectral domains where nearly total absorption can be achieved. (c) Full-wave simulations and analytical predictions for the absorption spectra (black lines) when backward illumination is applied to the array. We see that we have nearly perfect absorption at resonance. The period of the array is fixed to $a = 275$ nm.

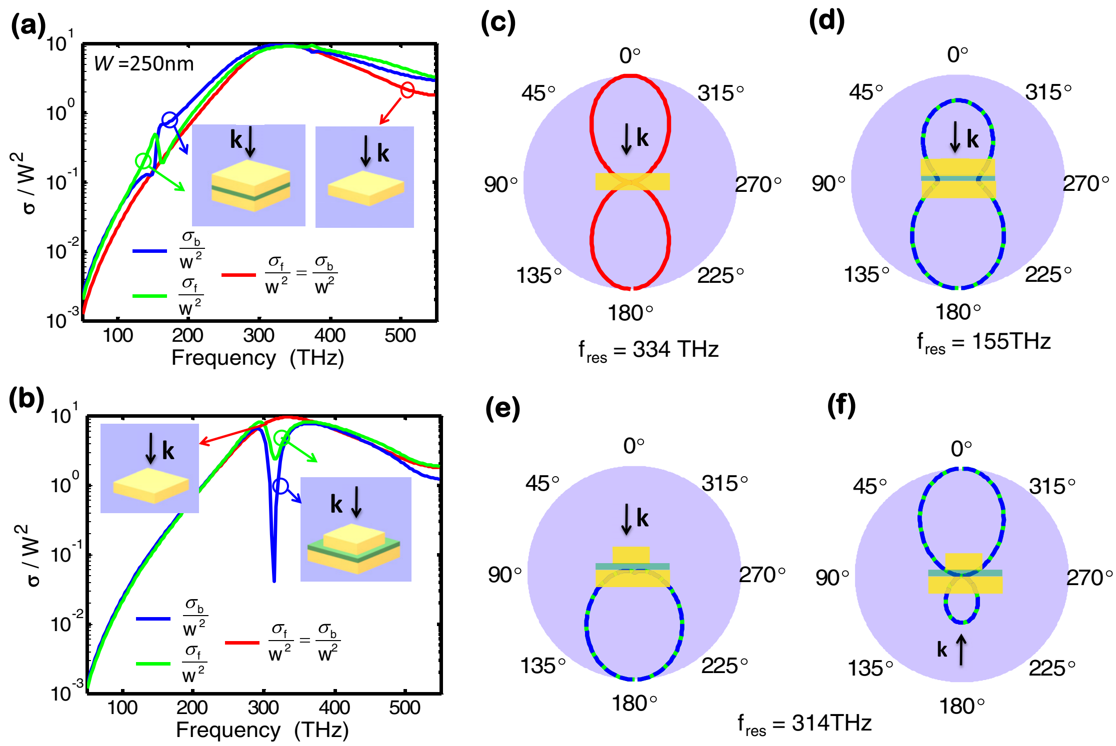

FIG. 4. (Color online) (a) and (b) Comparison between forward and backward frequency dependent normalized radar scattering cross sections for a single nanopatch (shown in red only since backward and forward radar scatterings are identical), two identical coupled nanopatches, and two nonidentical nanopatches (shown in green and blue) with $W_1/W_2 = 0.4$. Illumination occurs as shown in the inset. Electric field patterns of (c) a single nanopatch and (d) two identical coupled nanopatches at resonance. (e) and (f) Corresponding electric field patterns of two nonidentical coupled nanopatches for both backward and forward illumination directions at the resonance frequency, respectively.

their resonance strengths are 3–4 times smaller than the electric one at the desired wavelength.

It is worthwhile to mention that for an array made from wire omega particles the perfect absorption regime is unattainable since approaching the balance condition as detailed in [37] is practically impossible. In the present design, when moving from $\frac{W_1}{W_2} = 1$ (symmetric case) to smaller values the absorption increases very rapidly and exceeds the value of 90% at the ratio of $\frac{W_1}{W_2} \geqslant 0.8$ then approaches a maximum value of 94% at the optimum ratio of $\frac{W_1}{W_2} \approx 0.4$. Finally, it decreases very fast for ratios of $\frac{W_1}{W_2} \leqslant 0.3$ [blue curve in Fig. 3(c)]. This controllability makes our design an excellent candidate for frequency selective thin plasmonic nanosensors.

B. Directive nanoantenna with zero backscattering

In general, to have a nanoantenna with directive pattern, a balanced contribution of both electric and magnetic polarizabilities is sufficient; known as the first Kerker condition [59]. This condition can be achieved for meta-atoms without bianisotropy. However, having a meta-atom with a bianisotropic response adds at least two degrees of freedom. The first degree of freedom provides the ability to design an antenna which possesses different far field patterns when illuminated from opposite (forward and backward) directions. This means that one can design an antenna which shows a directive pattern for one direction but a nondirective pattern for the opposite direction [Figs. 4(e) and 4(f)]. The second relates to the fact that for some meta-atoms it is not possible to achieve the balance condition between the electric and magnetic polarizabilities. Therefore, breaking the symmetries of the meta-atoms will introduce an additional bianisotropy which might be a proper solution to easily satisfy the first Kerker condition. In the following we present these issues.

A bianisotropic antenna with zero backscattered field, possessing a directive pattern in the forward direction, for the backward illumination direction can be achieved if the backward radar scattering cross-section [58,61–63] σ_b, i.e.,

$$\sigma_b = \lim_{r\to\infty} 4\pi r^2 \frac{|E_{\rm sca}(\varphi = 0,\theta = 0)|^2}{|E_{\rm inc}|^2} = \frac{(\omega k_z)^2}{4\pi}\left|\eta\alpha_{xx}^{\rm ee} - \alpha_{xy}^{\rm em} + \alpha_{yx}^{\rm me} - \frac{1}{\eta}\alpha_{yy}^{\rm mm}\right|^2, \quad (8)$$

amounts to zero. Where $E_{\rm sca}$ and $E_{\rm inc}$ are the scattered and incident fields, respectively. Notice the forward radar scattering cross section reads as

$$\sigma_f = \lim_{r\to\infty} 4\pi r^2 \frac{|E_{\rm sca}(\varphi = 0,\theta = \pi)|^2}{|E_{\rm inc}|^2} = \frac{(\omega k_z)^2}{4\pi}\left|\eta\alpha_{xx}^{\rm ee} + \frac{1}{\eta}\alpha_{yy}^{\rm mm}\right|^2. \quad (9)$$

Figure 4 shows the scattered field for three different meta-atoms: a single nanopatch, two identical and nonidentical coupled nanopatches. It is obvious from Figs. 4(a) and 4(b) that the backscattered fields are canceled for two nonidentical coupled nanopatches at the design frequency (314 THz) while there is no cancellation for a single nanopatch as well as two identical coupled nanopatches. This cancellation is obviously a consequence of destructive interference between the electric and magnetic dipole moments [59,61,64–67]. It is important to mention that for the identical coupled nanopatches in the limit of dipole approximation [68] (small dielectric spacer, i.e., $g < 10$ nm) a zero backscattering regime is not achievable due to the fact that the electric and magnetic dipole moments cannot be in balance [Figs. 4(a) and 4(d)]. However, with the help of an additional electric quadrupole moment (larger dielectric spacer, e.g., $g = 50$ nm), it might be possible to realize a directive antenna with zero backscattering for the identical coupled nanopatches (not shown for brevity). Notice that the directive pattern occurs due to the coherent interference of the electric and magnetic dipoles as well as electric quadrupole [69].

Normalized polar field patterns at resonance are also plotted in Figs. 4(c)–4(f) to illustrate zero backscattering as well as the directivity of corresponding antennas. Notice that for the backscattering cancellation of fields both the strength and resonance frequency of the magnetoelectric coupling have to be tuned. The proposed design is a promising nominee for directive plasmonic antennas coupled to quantum emitters [70].

C. Conclusions

A simple design for a plasmonic metasurface formed by stacked nanopatches has been discussed. The fundamental feature of the proposed metasurface is its tunable bianisotropic response. It provides a handle on the electric, magnetic, and magnetoelectric responses. The magnetoelectric response corresponds to that of a planar array of omega particles (whose realization from a piece of wire has been known for the microwave range). The technical solution mimicking the omega particle by a pair of separated elements allows the so-called electromagnetic balance, i.e., the equivalence of the electric and magnetic polarizations of the metasurface. At visible frequencies, this balance has been earlier achieved only for nonbianisotropic metasurfaces (between the electric and magnetic Mie resonances of silicon spheres or spheroids). In the present case the amplitudes of three collective polarizabilities—electric, magnetic, and electromagnetic—can be engineered with the same strength. The presence of the bianisotropic response allows the asymmetry of reflectance for the illumination of the metasurface from opposite directions. A very strong asymmetry of reflection as well as nearly perfect absorption for the suggested effective omega metasurface have been shown. Moreover, a single element of this metasurface can operate as a very directive nanoantenna with zero backscattered fields (Huygens' scatterer).

The presence of easily controllable bianisotropy at optical frequencies can be useful for many applications: polarizers and polarization transformers, frequency selective absorbers, reflect arrays, transmit arrays based on so-called Huygens' surfaces, etc. The proposed solution can inspire researchers to design other meta-atoms possessing different types of bianisotropy.

ACKNOWLEDGMENTS

This work was supported by the Bundesministerium für Bildung und Forschung Thüringer Ministerium für Bildung, Wissenschaft und Kultur Deutsche Forschungsgemeinschaft.

[1] J. B. Pendry, Phys. Rev. Lett. **85**, 3966 (2000).
[2] A. V. Kildishev, A. Boltasseva, and V. M. Shalaev, Science **339** 6125 (2013).
[3] C. L. Holloway, M. A. Mohamed, E. F. Kuester, and A. Dienstfrey, IEEE Trans. Electromagn. Compatibility **47**, 853 (2005).
[4] C. L. Holloway, E. F. Kuester, and A. Dienstfrey, IEEE Antennas Wireless Propag. Lett. **10**, 1507 (2011).
[5] E. F. Kuester, M. A. Mohamed, M. Piket-May, and C. L. Holloway, IEEE Trans. Antennas Propag. **51**, 2641 (2003).
[6] F. Falcone, T. Lopetegi, M. A. G. Laso, J. D. Baena, J. Bonache, M. Beruete, R. Marqués, F. Martin, and M. Sorolla, Phys. Rev. Lett. **93**, 197401 (2004).
[7] Y. Zhao and A. Alù, Phys. Rev. B **84**, 205428 (2011).
[8] S. Sun, K.-Y. Yang, C.-M. Wang, T.-K. Juan, W. T. Chen, C. Y. Liao, Q. He, S. Xiao, W.-T. Kung, G.-Y. Guo *et al.*, Nano Lett. **12**, 6223 (2012).
[9] N. Yu and F. Capasso, Nat. Mater. **13**, 139 (2014).
[10] F. Aieta, P. Genevet, M. A. Kats, N. Yu, R. Blanchard, Z. Gaburro, and F. Capasso, Nano Lett. **12**, 4932 (2012).
[11] S. H. Mousavi, A. B. Khanikaev, and G. Shvets, Phys. Rev. B **85**, 155429 (2012).
[12] C. Saeidi and D. van der Weide, Appl. Phys. Lett. **103**, 183101 (2013).
[13] P.-Y. Chen and A. Alù, Phys. Rev. B **82**, 235405 (2010).
[14] M. Farmahini-Farahani and H. Mosallaei, Opt. Lett. **38**, 462 (2013).
[15] M. Albooyeh, D. Morits, and C. Simovski, Metamaterials **5**, 178 (2011).
[16] G. Dolling, C. Enkrich, M. Wegener, J. Zhou, C. M. Soukoulis, and S. Linden, Opt. Lett. **30**, 3198 (2005).
[17] V. M. Shalaev, Nat. Photon. **1**, 41 (2007).
[18] R. Alaee, C. Menzel, U. Huebner, E. Pshenay-Severin, S. Bin Hasan, T. Pertsch, C. Rockstuhl, and F. Lederer, Nano Lett. **13**, 3482 (2013).
[19] E. S. Barnard, J. S. White, A. Chandran, and M. L. Brongersma, Opt. Express **16**, 16529 (2008).
[20] D. Lehr, R. Alaee, R. Filter, K. Dietrich, T. Siefke, C. Rockstuhl, F. Lederer, E.-B. Kley, and A. Tünnermann, Appl. Phys. Lett. **105**, 143110 (2014).
[21] N. J. Halas, S. Lal, W.-S. Chang, S. Link, and P. Nordlander, Chem. Rev. **111**, 3913 (2011).
[22] T. Pakizeh and M. Käll, Nano Lett. **9**, 2343 (2009).
[23] M. Albooyeh and C. Simovski, J. Opt. **13**, 105102 (2011).

[24] N. Liu, H. Guo, L. Fu, S. Kaiser, H. Schweizer, and H. Giessen, Adv. Mater. **19**, 3628 (2007).
[25] C. Menzel, R. Alaee, E. Pshenay-Severin, C. Helgert, A. Chipouline, C. Rockstuhl, T. Pertsch, and F. Lederer, Opt. Lett. **37**, 596 (2012).
[26] M. Albooyeh, D. Morits, and S. A. Tretyakov, Phys. Rev. B **85**, 205110 (2012).
[27] F. G. De Abajo, Rev. Mod. Phys. **79**, 1267 (2007).
[28] L. Novotny, Phys. Rev. Lett. **98**, 266802 (2007).
[29] D. M. Pozar, *Microwave Engineering* (Wiley, New York, 2009).
[30] D.-H. Kwon and D. M. Pozar, IEEE Trans. Antennas Propag. **57**, 3720 (2009).
[31] C. Pfeiffer, N. K. Emani, A. M. Shaltout, A. Boltasseva, V. M. Shalaev, and A. Grbic, Nano Lett. **14**, 2491 (2014).
[32] C. Pfeiffer and A. Grbic, Phys. Rev. Lett. **110**, 197401 (2013).
[33] A. Serdyukov, *Electromagnetics of Bi-anisotropic Materials: Theory and Applications* (Taylor and Francis, London, 2001), Vol. 11.
[34] A. Kildishev, J. Borneman, X. Ni, V. Shalaev, and V. Drachev, Proc. IEEE **99**, 1691 (2011).
[35] A. Shaltout, V. Shalaev, and A. Kildishev, Opt. Express **21**, 21941 (2013).
[36] I. Sersic, M. A. van de Haar, F. B. Arango, and A. F. Koenderink, Phys. Rev. Lett. **108**, 223903 (2012).
[37] Y. Ra'di, V. S. Asadchy, and S. A. Tretyakov, IEEE Trans. Antennas Propag. **61**, 4606 (2013).
[38] C. Menzel, C. Helgert, C. Rockstuhl, E.-B. Kley, A. Tünnermann, T. Pertsch, and F. Lederer, Phys. Rev. Lett. **104**, 253902 (2010).
[39] T. Niemi, A. Karilainen, and S. Tretyakov, IEEE Trans. Antennas Propag. **61**, 3102 (2013).
[40] Y. Ra'di, V. S. Asadchy, and S. A. Tretyakov, Phys. Rev. B **89**, 075109 (2014).
[41] S. Tretyakov, *Analytical Modeling in Applied Electromagnetics* (Artech House, London, 2003).
[42] C. R. Simovski, M. S. Kondratjev, P. A. Belov, and S. A. Tretyakov, IEEE Trans. Antennas Propag. **47**, 1429 (1999).
[43] S. Mühlig, C. Menzel, C. Rockstuhl, and F. Lederer, Metamaterials **5**, 64 (2011).
[44] S. Weitemeyer, M. Husnik, and M. Wegener, Appl. Phys. Lett. **104**, 031111 (2014).
[45] F. Bernal Arango, T. Coenen, and A. F. Koenderink, ACS Photon. **1**, 444 (2014).
[46] P. Grahn, A. Shevchenko, and M. Kaivola, New J. Phys. **14**, 093033 (2012).
[47] P. Grahn, A. Shevchenko, and M. Kaivola, J. Eur. Opt. Soc. Rapid Publ. **8**, 13009 (2013).
[48] M. S. Kondratiev, C. R. Simovski, and P. A. Belov, in *5th Annual International Symposium on Smart Structures and Materials* (International Society for Optics and Photonics, Bellingham, WA, 1998), pp. 669–678.
[49] A. J. Viitanen, I. Hänninen, and S. Tretyakov, Progress Electromagn. Res. **38**, 97 (2002).
[50] Y. E. Terekhov, A. Zhuravlev, and G. Belokopytov, Moscow Univ. Phys. Bull. **66**, 254 (2011).
[51] V. S. Asadchy, I. A. Faniayeu, Y. Ra'di, and S. A. Tretyakov, Photon. Nanostruct. Fund. Appl. **12**, 298 (2014).
[52] C. Rockstuhl, C. Menzel, S. Mühlig, J. Petschulat, C. Helgert, C. Etrich, A. Chipouline, T. Pertsch, and F. Lederer, Phys. Rev. B **83**, 245119 (2011).
[53] C. Simovski, S. Tretyakov, A. Sochava, B. Sauviac, F. Mariotte, and T. Kharina, J. Electromagn. Waves. Appl. **11**, 1509 (1997).
[54] N. I. Landy, S. Sajuyigbe, J. J. Mock, D. R. Smith, and W. J. Padilla, Phys. Rev. Lett. **100**, 207402 (2008).
[55] K. Aydin, V. E. Ferry, R. M. Briggs, and H. A. Atwater, Nat. Commun. **2**, 517 (2011).
[56] C. M. Watts, X. Liu, and W. J. Padilla, Adv. Mater. **24**, OP98 (2012).
[57] R. Alaee, C. Menzel, C. Rockstuhl, and F. Lederer, Opt. Express **20**, 18370 (2012).
[58] S. Person, M. Jain, Z. Lapin, J. J. Sáenz, G. Wicks, and L. Novotny, Nano Lett. **13**, 1806 (2013).
[59] M. Kerker, D.-S. Wang, and C. Giles, J. Opt. Soc. Am. A **73**, 765 (1983).
[60] E. Poutrina, A. Rose, D. Brown, A. Urbas, and D. R. Smith, Opt. Express **21**, 31138 (2013).
[61] B. Luk'yanchuk, N. I. Zheludev, S. A. Maier, N. J. Halas, P. Nordlander, H. Giessen, and C. T. Chong, Nat. Mater. **9**, 707 (2010).
[62] I. V. Lindell, A. Sihvola, P. Yla-Oijala, and H. Wallén, IEEE Trans. Antennas Propag. **57**, 2725 (2009).
[63] J. Vehmas, Y. Ra'di, A. O. Karilainen, and S. A. Tretyakov, IEEE Trans. Antennas Propag. **61**, 3747 (2013).
[64] L. Wei, A. E. Miroshnichenko, and Y. S. Kivshar, Chin. Phys. B **23**, 047806 (2014).
[65] I. Staude, A. E. Miroshnichenko, M. Decker, N. T. Fofang, S. Liu, E. Gonzales, J. Dominguez, T. S. Luk, D. N. Neshev, I. Brener *et al.*, ACS Nano **7**, 7824 (2013).
[66] A. I. Kuznetsov, A. E. Miroshnichenko, Y. H. Fu, J. Zhang, and B. Lukyanchuk, Sci. Rep. **2**, 492 (2012).
[67] S. N. Sheikholeslami, A. García-Etxarri, and J. A. Dionne, Nano Lett. **11**, 3927 (2011).
[68] C. Menzel, E. Hebestreit, R. Alaee, M. Albooyeh, S. Mühlig, S. Burger, C. Rockstuhl, C. Simovski, S. Tretyakov, F. Lederer *et al.*, Phys. Rev. B **89**, 155125 (2014).
[69] I. M. Hancu, A. G. Curto, M. Castro-López, M. Kuttge, and N. F. van Hulst, Nano Lett. **14**, 166 (2013).
[70] A. G. Curto, G. Volpe, T. H. Taminiau, M. P. Kreuzer, R. Quidant, and N. F. van Hulst, Science **329**, 930 (2010).